Proton vs. neutron captures in the neutrino winds of core-collapse supernovae

S. Wanajo[1,2], H.-T. Janka[2], B. Müller[2], and S. Kubono[3]

[1]Technische Universität München, Excellence Cluster Universe, Boltzmannstr. 2, D-85748 Garching, Germany
[2]Max-Planck-Institut für Astrophysik, Karl-Schwarzschild-Str. 1, D-85748 Garching, Germany
[3]Center for Nuclear Study, University of Tokyo, RIKEN Campus, 2-1 Hirosawa, Wako, Saitama 351-0198, Japan

E-mail: shinya.wanajo@universe-cluster.de

Abstract. Recent one-dimensional (1D) hydrodynamical simulations of core-collapse supernovae (CCSNe) with a sophisticated treatment of neutrino transport indicate the neutrino-driven winds being proton-rich all the way until the end of their activity. This seems to exclude all possibilities of neutron-capture nucleosynthesis, but provide ideal conditions for the νp-process, in neutrino winds. New 2D explosion simulations of electron-capture supernovae (ECSNe; a subset of CCSNe) exhibit, however, convective neutron-rich lumps, which are absent in the 1D case. Our nucleosynthesis calculations indicate that these neutron-rich lumps allow for interesting production of elements between iron group and $N = 50$ nuclei (Zn, Ge, As, Se, Br, Kr, Rb, Sr, Y, Zr, with little Ga). Our models do not confirm ECSNe as sources of the strong r-process (but possibly of a weak r-process up to Pd, Ag, and Cd in the neutron-rich lumps) nor of the νp-process in the subsequent proton-rich outflows. We further study the νp-process with semi-analytic models of neutrino winds assuming the physical conditions for CCSNe. We also explore the sensitivities of some key nuclear reaction rates to the nucleosynthetic abundances. Our result indicates that the νp-process in CCSNe (other than ECSNe) can be the origin of p-nuclei up to $A = 108$, and even up to $A = 152$ in limiting conditions.

1. Introduction

The astrophysical origin of nuclei beyond iron is still far from understanding. In particular, the stellar sources of half the heavy nuclei that cannot be synthesized by the s(low neutron-capture)-process remain a mystery. The residual nuclei, subtracting the s-process components from the solar system abundances heavier than iron, are generally assigned to either the r(apid neutron-capture)-process or the p-process. The latter produces the p(roton)-rich isotopes that cannot be synthesized either by s- or r-processes. In the past decades, the proto-neutron-star (PNS) winds (or neutrino winds) [1-7] and the shocked O/Ne layers [8-10] of core-collapse supernovae (CCSNe) have been proposed as the promising sources of r- and p-nuclei (by the γ-process), respectively.

Recent one-dimensional (1D) hydrodynamic studies of core-collapse supernovae with sophisticated neutrino transport taken into account suggest, however, that the neutrino-driven ejecta are p-rich all the way until the end of the wind activity [11, 12]. This seems to exclude the possibility of r-processing in the neutrino winds of CCSNe. The γ-process scenario also has a severe problem in producing some light p-nuclei, in particular ^{92,94}Mo and ^{96,98}Ru [9].

Published under licence by IOP Publishing Ltd

Multi-dimensionality changes the above situation for the early neutrino-driven ejecta. New self-consistent 2D explosion simulations of electron-capture supernovae (ECSNe; a subset of CCSNe arising from collapsing O-Ne-Mg cores) exhibit n(eutron)-rich lumps of matter being dredged up by convective overturn from the outer layers of the PNS during the early stages of the explosion (Müller, Janka, & Kitaura, in preparation), a feature that is absent in the 1D situation. This allows for interesting production of elements beyond iron in nuclear statistical equilibrium (NSE), by α-processing, and potentially by weak r-processing [13]. The situation is similar to the 1D case once the initial convective material has been swept away from the PNS surface. No r-process is expected in the later p-rich winds.

The p-rich winds of CCSNe from more massive progenitors provide, however, ideal physical conditions for the νp-process, a recently discovered nucleosynthetic process [14-17]. Tiny amounts of free neutrons arising from $\bar{\nu}_e$ capture on free protons in a neutrino wind give rise to neutron capture on the β^+-waiting-point nuclei along the classical rp-process pathway (e.g., ^{64}Ge with a β^+-decay half-life of $\sim$ 1 min), bypassing these waiting points. Recent studies suggest that the p-nuclei up to $A \sim 110$, including ^{92,94}Mo and ^{96,98}Ru, can be produced in neutrino winds of CCSNe by the νp-process within reasonable ranges of the model parameters [16, 17].

In this article, we outline our recent results of nucleosynthesis studies on the basis of self-consistent 2D models of ECSNe [13] and semi-analytic wind models for CCSNe [18], aiming at identifying the origins of nuclei beyond iron. In the studies of ECSNe, the nucleosynthetic abundances are compared with those from the 1D counterpart in our previous study [19]. The sensitivity of the nucleosynthetic yields on the minimum Y_e (electron fraction or the number of protons per baryon) in n-rich lumps, $Y_\mathrm{e,min}$, is also examined to investigate whether ECSNe can lead to an r-process. In the neutrino-wind studies, nucleosynthesis calculations are performed for wide ranges of wind-termination radii r_wt and Y_e. Sensitivities on the crucial reaction rates, triple-α and $^{56}\mathrm{Ni}(n,p)^{56}\mathrm{Co}$, are also discussed.

2. Nucleosynthesis in the early ejecta of Electron-capture Supernovae

The nucleosynthesis analysis made use of about 2000 representative tracer particles, by which the thermodynamic histories of ejecta chunks were followed in our 2D hydrodynamic calculation of an ECSN. The model was computed with a sophisticated (ray-by-ray-plus) treatment of the energy-dependent neutrino transport, using the Prometheus-Vertex code and the same microphysics (weak-interaction rates, nuclear burning treatment, and nuclear equation of state of [20]) as in its 1D counterpart [21]. Some aspects of the 2D model in comparison to 1D results were discussed by [22].

The pre-collapse model of the O-Ne-Mg core emerged from the evolution of an $8.8\,M_\odot$ star [23]. Because of the very steep density gradient near the core surface, the shock expands continuously, and a neutrino-powered explosion sets in at $t \sim 100$ ms p.b. in 1D and 2D essentially in the same way and with a very similar energy ($\sim 10^{50}$ erg) [22].

In the multi-dimensional case, however, the negative entropy profile created by neutrino heating around the PNS leads to a short phase of convective overturn, in which accretion downflows deleptonize strongly, are neutrino heated near the neutrinosphere, and rise again quickly, accelerated by buoyancy forces. Thus n-rich matter with modest entropies per nucleon ($s \sim$13–15 k_B; k_B is Boltzmann's constant) gets ejected in mushroom-shaped structures typical of Rayleigh-Taylor instability. Figure 1 displays the situation 262 ms after bounce when the pattern is frozen in and self-similarly expanding.

As a consequence, the mass distribution of the ejecta in the 2D model extends down to $Y_\mathrm{e,min}$ as low as $\sim$0.4, which is significantly more n-rich than in the corresponding 1D case ($Y^\mathrm{1D}_\mathrm{e,min} \sim 0.47$). Figure 2 shows the Y_e-histograms at the end of the simulations. The total ejecta masses are $1.39 \times 10^{-2}\,M_\odot$ for the 1D model and $1.14 \times 10^{-2}\,M_\odot$ in 2D, where

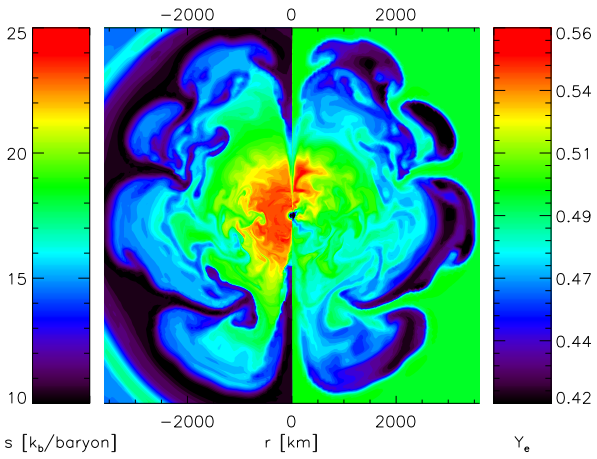

Figure 1. Snapshot of the convective region of the 2D simulation of an ECSN at 262 ms after core bounce with entropy per nucleon (s; left) and Y_e (right).

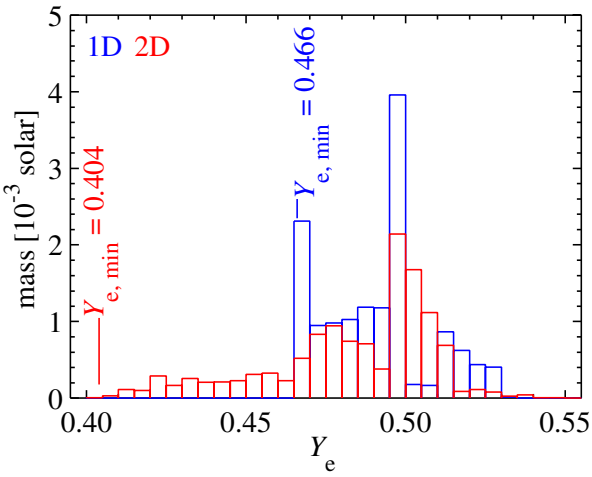

Figure 2. Ejecta masses vs. Y_e for the 1D (blue) and 2D (red) explosion models. The width of a Y_e-bin is chosen to be $\Delta Y_\mathrm{e} = 0.005$.

the difference is partly due to the different simulation times, being ∼800 ms and ∼400 ms, respectively (core bounce occurs at ∼50 ms). However, the ejecta after ∼250 ms p.b. are only proton-rich, contributing merely to the $Y_\mathrm{e} > 0.5$ side in Fig. 2.

The nucleosynthetic yields are obtained with the reaction network code (including neutrino interactions) described in [19]. Using thermodynamic trajectories directly from the 2D ECSN model, the calculations are started when the temperature decreases to 9×10^9 K, assuming initially free protons and neutrons with mass fractions Y_e and $1 - Y_\mathrm{e}$, respectively. The final abundances for all isotopes are obtained by mass-integration over all 2000 marker particles.

The resulting *elemental* mass fractions relative to solar values [24], or the production factors, are shown in Fig. 3 (red) compared to the 1D case (blue) from [19]. The "normalization band" between the maximum (367 for Sr) and a tenth of that is indicated in yellow with the medium marked by a dotted line. The total ejecta mass is taken to be the sum of the ejected mass from the core and the outer H/He-envelope ($= 8.8\,M_\odot - 1.38\,M_\odot + 0.0114\,M_\odot = 7.43\,M_\odot$). Note that the $N = 50$ species, ^{86}Kr, ^{87}Rb, ^{88}Sr, and ^{90}Zr, have the largest production factors for *isotopes* with values of 610, 414, 442, and 564, respectively.

As discussed by [19], in the 1D case only Zn and Zr are on the normalization band, although some light p-nuclei (up to ^{92}Mo) can be sizably produced. In contrast, we find that all elements between Zn and Zr, except for Ga, fall into this band in the 2D case (Ge is marginal), although all others are almost equally produced in 1D and 2D. This suggests ECSNe to be likely sources of Zn, Ge, As, Se, Br, Kr, Rb, Sr, Y, and Zr, in the Galaxy. Note that the origin of these elements is not fully understood, although Sr, Y, and Zr in the solar system are considered to be dominantly made by the s-process. The ejected masses of ^{56}Ni ($\rightarrow^{56}$Fe; $3.0 \times 10^{-3}\,M_\odot$) and all Fe ($3.1 \times 10^{-3}\,M_\odot$) are the same as in the 1D case ($2.5 \times 10^{-3}\,M_\odot$) [19].

The fact that oxygen is absent in ECSN ejecta but a dominant product of more massive CCSNe, can pose a constraint on the frequency of ECSNe [19]. Considering the isotope ^{86}Kr with its largest production factor in our 2D model and assuming f to be the fraction of ECSNe relative to all CCSNe, one gets

$$\frac{f}{1-f} = \frac{X_\odot(^{86}\mathrm{Kr})/X_\odot(^{16}\mathrm{O})}{M(^{86}\mathrm{Kr})/M_\mathrm{noEC}(^{16}\mathrm{O})} = 0.050, \qquad (1)$$

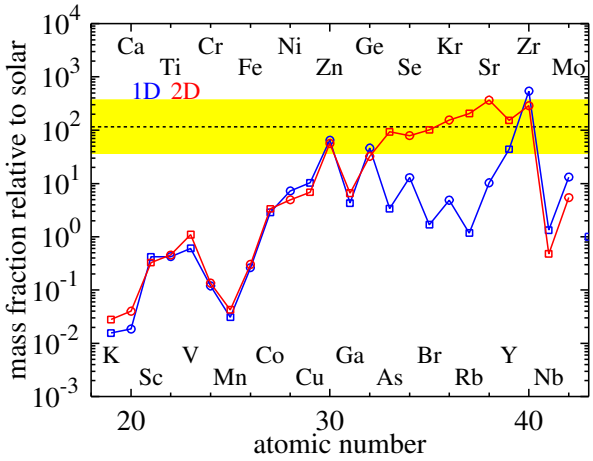

Figure 3. Elemental mass fractions in the ECSN ejecta relative to solar values [24], comparing the 2D results (red) with the 1D counterpart (blue) from [19]. The normalization band (see text) is marked in yellow.

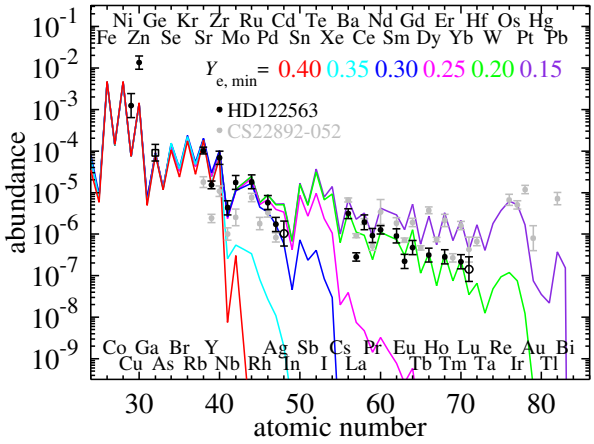

Figure 4. Elemental abundances for various $Y_{e,min}$ compared with the stellar abundances of the r-process deficient star HD 122563 with [Fe/H] ≈ -2.7 [30, 32, 33] and the r-process enhanced star CS 22892-052 with [Fe/H] ≈ -3.1 [34].

where $X_\odot(^{86}\mathrm{Kr}) = 2.4 \times 10^{-8}$ and $X_\odot(^{16}\mathrm{O}) = 6.6 \times 10^{-3}$ are the mass fractions in the solar system [24], $M(^{86}\mathrm{Kr}) = 1.1 \times 10^{-4}\,M_\odot$ is our ejecta mass of ^{86}Kr, and $M_{\mathrm{noEC}}(^{16}\mathrm{O}) = 1.5\,M_\odot$ the production of ^{16}O by all other CCSNe, averaged over the stellar initial mass function between $13\,M_\odot$ and $40\,M_\odot$ (see [19, 25]). Equation (1) leads to $f = 0.048$. The frequency of ECSNe relative to all CCSNe is thus ∼4%, assuming that all ^{86}Kr in the solar system except for a possible contribution from the s-process (18%, [26]), originates from ECSNe. This is in good agreement with the prediction from a recent synthetic model of super asymptotic-giant-branch stars (for solar metallicity models, [27]).

The remarkable difference between the 1D and 2D cases (Fig. 3) can be understood by the combined element formation in nuclear statistical equilibrium (NSE) and through the α-process (or "n-rich, α-rich freezeout from NSE", [28]). The α-process makes nuclei heavier than the Fe-group up to $A \sim 100$. ^{64}Zn, ^{88}Sr, and ^{90}Zr are thus produced at $Y_\mathrm{e} = 0.43$–0.49. The α-process, however, is known to leave a deep trough in the abundance curve between A ∼60 and 90 because of the strong binding at $N = 28$ and 50. This explains the substantial underproduction of elements around Z ∼33–37 in the 1D case (Fig. 3, blue line).

Since NSE with neutron excess ($Y_\mathrm{e} \sim 0.4$) leads to nuclei heavier than the Fe-group up to $A \approx 84$ (see, e.g., [29]), the trough can be filled by NSE-abundances assembled in the n-rich ejecta lumps. Accordingly, NSE in the Y_e-range of 0.40–0.42 yields substantial amounts of species with $A = 74$–84, nuclei that cannot be created by the α-process.

In the n-rich ejecta lumps NSE-like conditions are established for several reasons. They have smaller entropies ($s \approx 13$–$15\,k_\mathrm{B}$ per baryon) than the other ejecta (where $s \approx 15$–$20\,k_\mathrm{B}$ per baryon; Fig. 1). This favors α-particles to disappear when NSE ends as the temperature drops. In addition, the α's become easily locked up and tightly bound in nuclei, i.e., their separation energies are large (cf., e.g., Fig. 1b in [28]), because nuclei with n-excess do not readily release α's to move farther away from β-stability.

Our results also imply that ECSNe can be the source of Sr, Y, and Zr as observed in r-process deficient Galactic halo stars (Fig. 4). A number of such stars with detailed abundance determinations indicate, however, a possible link with the elements beyond $N = 50$, e.g. Pd and

Ag [30, 31]. Our ECSN models cannot account for the production of such elements, but in their ejecta a small change of Y_e can drastically change the nucleosynthesis [19]. Due to limitations of the numerical resolution and the lack of the third dimension, or some sensitivity to the nuclear equation of state, it cannot be excluded that ECSNe also eject tiny amounts of matter with $Y_{e,min}$ slightly lower than predicted by the 2D simulation.

We therefore compare the nucleosynthesis for $Y_{e,min} = 0.40$ of our ECSN model and for artificially reduced values of $Y_{e,min} = 0.35, 0.30, 0.25, 0.20$, and 0.15 with the abundance patterns of representative r-process deficient (HD 122563, [30, 32, 33]) and enhanced (CS 22892-052, [34]) stars (Fig. 4). For that we use the thermodynamic trajectory of the lowest Y_e (= 0.404) of the original model but apply Y_e down to 0.15 in steps of $\Delta Y_e = 0.005$. The ejecta masses in these additional Y_e-bins are chosen to be constant with $\Delta M = 2 \times 10^{-5}\, M_\odot$ in the cases $Y_{e,min} = 0.35$ and 0.30, and $\Delta M = 10^{-5}\, M_\odot$ for the other $Y_{e,min}$.

Figure 4 shows that $Y_e \leq 0.35$ is needed to obtain elements beyond $N = 50$. A remarkable agreement with the abundance pattern in HD 122563 up to Cd ($Z = 48$) can be seen for $Y_{e,min} = 0.30$. Such a mild reduction of $Y_{e,min}$ in the ECSN ejecta is well possible for the reasons mentioned above. A reasonable match of the heavier part beyond $Z = 48$ requires $Y_{e,min} \approx 0.20$. This, however, leads to a poor agreement for Ag and Cd. We therefore speculate that ECSNe could be the sources of the elements up to Cd in r-process deficient stars, and the heavier elements are from a different origin. Moreover, $Y_{e,min} = 0.15$ is necessary to reproduce the abundance pattern of r-process enhanced stars like CS 22892-052. Such a low Y_e seems out of reach and disfavors ECSNe as production sites of heavy r-process nuclei.

We note that the neutron-capture reactions start from seeds with $A \sim 80$ formed in NSE-like conditions, not from the α-processed seeds ($A \sim$ 90–100). We therefore prefer to call the described process producing the elements beyond $N = 50$, presumably up to Cd, "weak r-process" [35, 30] rather than α-process or charged-particle process [28, 36].

Our present calculations are limited to the first $\leq$400 ms after bounce and do not include the neutrino-driven PNS wind. The latter, however, turned out to have proton excess in 1D models of the long-term evolution of ECSNe [12]. It thus makes only p-rich isotopes as discussed in § 3 and has no effect on the discussed results in this section.

3. Nucleosynthesis in the Proton-rich Neutrino Winds of Core-collapse Supernovae

The neutrino-driven outflows are found to be p-rich after the early convective lumps have been ejected from the PNS vicinity [11, 12]. In this section, the thermodynamic trajectories of such outflows are obtained using a semi-analytic, spherically symmetric, general relativistic model of neutrino-driven winds. This model has been developed in previous r-process [6, 37-39] and νp-process [17] studies. Here, we describe several modifications added to the previous version.

The equation of state for ions (ideal gas) and arbitrarily degenerate, arbitrarily relativistic electrons and positrons is taken from [40]. The root-mean-square averaged energies of neutrinos are taken to be 12, 14, and 14 MeV, for electron, anti-electron, and the other types of neutrinos, respectively, in light of a recent self-consistently exploding models of ECSNe [21, 12, 41]. These values are consistent with other recent studies for more massive progenitors [11]. The mass ejection rate $\dot{M}$ at the neutrinosphere is determined such that the outflow becomes supersonic (i.e., *wind*) through the sonic point.

The neutron star mass M_{ns} is taken to be $1.4\, M_\odot$ (see [18] for the dependence on M_{ns}). The radius of the neutrinosphere is assumed to be $R_\nu(L_\nu) = (R_{\nu 0} - R_{\nu 1})(L_\nu / L_{\nu 0}) + R_{\nu 1}$ as a function of the neutrino luminosity L_ν (taken to be the same for all the flavors), where $R_{\nu 0} = 30$ km, $R_{\nu 1} = 10$ km, and $L_{\nu 0} = 10^{52.6} = 3.98 \times 10^{52}$ ergs s^{-1}. This roughly mimics the evolution of R_ν in recent hydrodynamic simulations (e.g., [42]). The wind solution is obtained with $L_\nu = 1 \times 10^{52}$ erg s^{-1} ($R_\nu = 12.5$ km; see [18] for the dependence on L_ν). The time variations of radius r from the center, density ρ, and temperature T are shown in Figure 1 (black line). The

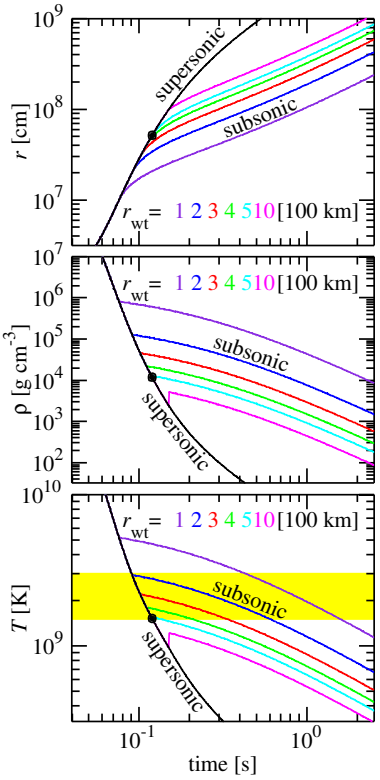

Figure 5. Radius (top), density (middle), and temperature (bottom) as a function of time (set to 0 at the neutrino sphere) for $M_{\rm ns} = 1.4\,M_\odot$ and $L_\nu = 1 \times 10^{52}$ erg s^{-1}.

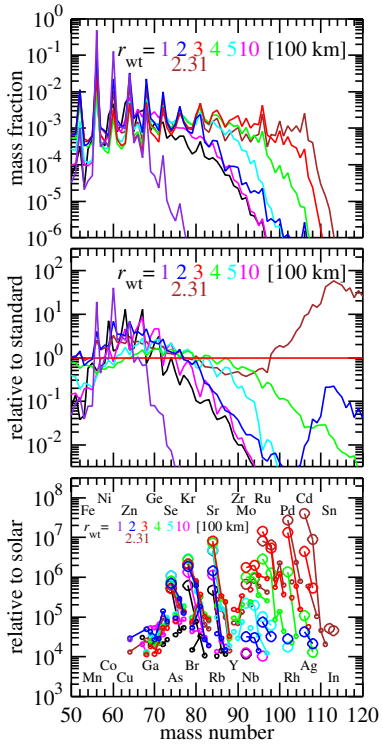

Figure 6. Nucleosynthetic abundances for various $r_{\rm wt}$ (top), their ratios relative to those for the standard model (middle), and relative to solar values (bottom).

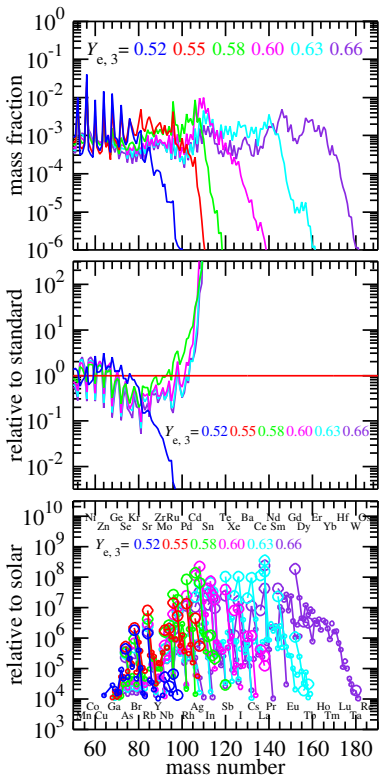

Figure 7. Same as Figure 6, but for $Y_{\rm e,3}$.

time variations after the wind-termination by the preceding supernova ejecta are calculated as described in [18]. The curves for different wind-termination radii, $r_{\rm wt}$, are shown in Figure 5. The nucleosynthetic abundances in the neutrino-driven outflows are calculated as the same way in § 2.

We first explore the effect of the wind-termination due to the preceding slowly outgoing ejecta [43, 44] on the νp-process. The termination point is located at $r_{\rm wt} = 100$, 200, 231, 300 (standard model), 400, 500, and 1000 km on the transonic wind trajectory (black line) shown in Figure 5 (top panel). For the initial compositions, $Y_{\rm e} = 0.600$ is taken. The result of nucleosynthesis calculations is shown in Figure 6. The top panel shows the mass fractions of nuclei as a function of atomic mass number, A. We find that the case with $r_{\rm wt} = 231$ km has the maximum efficiency of producing nuclei with $A \sim 100$–110 (including our calculations not shown here). The middle and bottom panels show, respectively, the mass fractions relative to the standard model and to solar values [24], i.e., production factors. We find a noticeable effect of wind termination on the νp-process; the production of p-nuclei between $A = 90$ and 110 is outstanding for the cases with $r_{\rm wt} = 231$ and 300 km (standard model).

Given that our standard model represents a typical supernova condition, this implies that the νp-process can be the source of the solar p-abundances up to $A = 108$ (^{108}Cd). However, this favorable condition is not robust against a variation of $r_{\rm wt}$ (and thus the temperature at $r = r_{\rm wt}$, $T_{\rm wt}$); the outflows with $r_{\rm wt} = 200$ km ($T_{\rm wt,9} = 2.95$; in units of 10^9 K) and $r_{\rm wt} \geq 500$ km

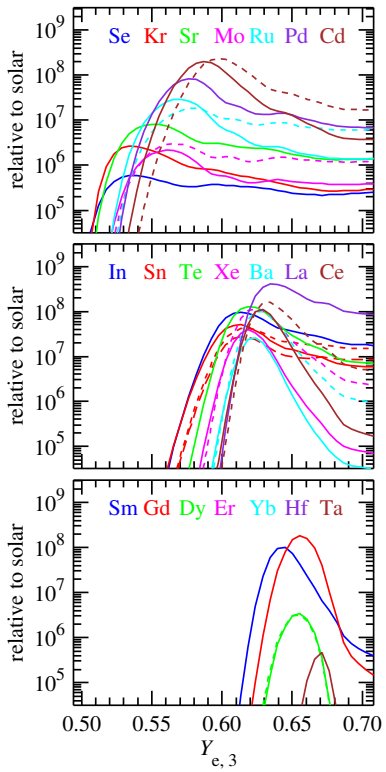

Figure 8. Nucleosynthetic p-abundances relative to solar values as a function of $Y_{e,3}$.

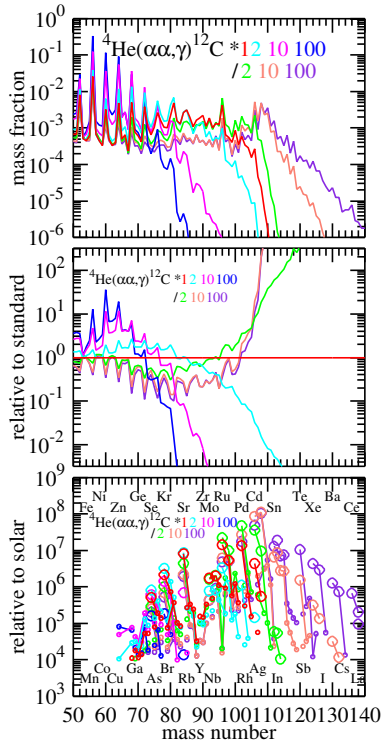

Figure 9. Same as Figure 6, but for variations on the triple-α reaction.

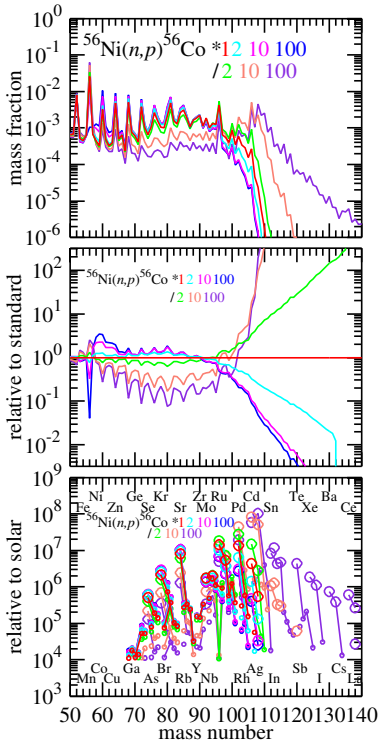

Figure 10. Same as Figure 6, but for variations on the ^{56}Ni$(n,p)^{56}$Co reaction.

($T_{\rm wt,9} < 1.55$) end up with the maximum mass number of $A_{\rm max} = 84$ (^{84}Sr). Note that the outflow with $r_{\rm wt} = 1000$ km leads to a similar result as that without wind termination (black line in Figure 2). This indicates that the role of wind termination is unimportant for $T_{\rm wt,9} < 1.5$. We find no substantial νp-processing for the outflow with $r_{\rm wt} = 100$ km, either (Figure 6). This is due to the substantially smaller $Y_{\rm e}$ at the beginning of the νp-process (defined at 3×10^9 K), $Y_{\rm e,3} = 0.509$ (only slightly p-rich), than those for the other cases (0.550). Noted that $Y_{\rm e,3}$ is always lower than its initial $Y_{\rm e}$ ($= 0.600$ in the present cases) owing to neutrino effects [18].

In summary, our exploration here elucidates a crucial role of wind termination on the νp-process. On one hand, a fast expansion above the temperature $\sim 3 \times 10^9$ K (more precisely, 2.65×10^9 K in the present condition) is favored to obtain a high proton-to-seed ratio at the onset of the νp-process. On the other hand, a slow expansion below this temperature, owing to wind termination, is needed for efficient νp-processing. The reason for negligible production of p-nuclei in ECSNe [19, 13] is likely due to their large $r_{\rm wt}$ resulting from a fast explosion [21, 22].

Besides wind termination, $Y_{\rm e}$ is obviously one of the most important ingredients in the νp-process as it controls the p-richness in the ejecta. Recent hydrodynamical studies with elaborate neutrino transport indicate that $Y_{\rm e}$ exceeds 0.5 and increases up to ~ 0.6 during the neutrino-driven wind phase [11, 12]. It should be noted that $Y_{\rm e}$ substantially decreases from its initial value owing to the neutrino effects. In our standard model, the value decreases from $Y_{\rm e} = 0.600$ (at 9×10^9 K) to $Y_{\rm e,3} = 0.550$ at the onset of the νp-process (3×10^9 K). However, these neutrino effects would highly dependent on the neutrino luminosities and energies of electron and anti-electron neutrinos assumed in this study. We thus take the value at the onset of the νp-process, $Y_{\rm e,3}$, as a reference.

Figure 7 shows the nucleosynthetic results for $Y_{e,3} = 0.523, 0.550, 0.576, 0.603, 0.629$, and 0.655. The value of r_{wt} (and thus T_{wt}) is kept to be 300 km (2.19×10^9 K). We find a great impact of the Y_e variation; an increase of only $\Delta Y_{e,3} \sim 0.03$ leads to a 10-unit increase of A_{max}, while the production factors are similar for $Y_{e,3} > 0.550$. The production factor for each p-nucleus is also displayed in Figure 8 as a function of $Y_{e,3}$. Each element is color coded with the solid, dashed, and long-dashed lines for the lightest, second-lightest, and third-lightest (^{115}Sn is only the case) isotopes, respectively. We find in the top panel that the p-nuclei up to $A = 108$ (^{108}Cd) take the maximum overproduction factors between $Y_{e,3} = 0.53$ and 0.60. Given the maximum $Y_{e,3}$ to be ~ 0.6 according to recent hydrodynamic results [11, 12], this implies that the maximum mass number of the p-nuclei produced by the νp-process is $A = 108$ (^{108}Cd).

In principle, the heavier p-nuclei can be synthesized if the matter is more proton-rich than $Y_{e,3} = 0.6$. The middle panel of Figure 8 shows that the overproduction factors of the p-nuclei from $A = 113$ (^{113}In) up to $A = 138$ (^{138}Ce) are maximal between $Y_{e,3} = 0.61$ and 0.63. Furthermore, ^{144}Sm and ^{152}Gd reach the maximum overproduction factors at $Y_{e,3} = 0.64$ and 0.66, respectively (bottom panel in Figure 8). The end point of the νp-process appears to be at $A \sim 180$ (^{180}Ta) in our explored cases. It should be noted that the wind-termination plays a crucial role as well. The p-nuclei heavier than $A = 140$ cannot be produced at all without wind termination [18].

There have been continuing experimental works relevant to the νp-process (e.g., [45]) since its discovery. However, we still rely upon theoretical or old experimental estimates for the vast majority of nuclear reactions accompanied with the νp-process, which may suffer from large uncertainties. Here, we test the effect of possible uncertainties in triple-α and ^{56}Ni$(n,p)^{56}$Co reactions by multiplying or dividing their original values by factors of 2, 10, and 100 with the standard model. The former and the latter are taken to be the key reactions as for the seed (^{56}Ni) production and the starting point of the νp-process, respectively (see [18] for other rates).

The result for the triple-α reaction is shown in Figure 9, where the forward and inverse rates are multiplied or divided by the same factors. We find substantial changes in the production of p-nuclei with $A \sim 100$–110 for a factor of 2 variation on the rate, and more drastic changes for a greater factor variation. The reason can be mainly attributed to the resulting proton-to-seed ratio. A larger triple-α rate leads to a more efficient seed production and thus a smaller proton-to-seed ratio. A larger rate during the νp-process phase also yields more carbon and other intermediate-mass nuclei that act as *proton poison*. As a result, efficiency of the νp-process decreases. The same interpretation is applicable to the opposite case with a smaller rate.

We also find a remarkable change in the p-abundances with $A \sim 110$ by a factor of 10 with only a factor of 2 variation on ^{56}Ni$(n,p)^{56}$Co (Figure 10). This demonstrates that the (n,p) reaction on the first (n,p)-*waiting nucleus* ^{56}Ni plays a key role for the progress of nuclear flow. It should be noted that a smaller rate results in larger production factors and A_{max} as can be seen in the bottom panel of Figure 10. This is a consequence of the nuclear flow stagnating at ^{96}Pd ($N = 50$ and $Z = 46$) before reaching $Z = 50$, because of the shell-closure for neutrons. As a result, ^{96}Pd plays a role of the "seed" nucleus for producing nuclei heavier than $A = 96$. For the standard model, free protons and neutrons are also consumed by the nuclei lighter than $A = 96$ with similar abundances (Figure 10; top panel), which are continuously supplied by the flow starting from ^{56}Ni. In contrast, the reduced ^{56}Ni$(n,p)^{56}$Co rate leads to the smaller abundances of nuclei between $A = 56$ and 96. Therefore, a larger number of free protons and neutrons are available for the "seed" nuclei ^{96}Pd.

4. Summary

Using ejecta-mass tracers from a self-consistent 2D explosion model and wind trajectories from a semi-analytic PNS wind model, we computed the nucleosynthesis in the early ejecta of ECSNe and in the p-rich neutrino-driven outflows of CCSNe. Our results are summarized as follows

(see [18, 13] for more detail).

The n-rich lumps in the early ECSN ejecta with Y_e down to 0.4, which are absent in more massive CCSNe (e.g., [42]), allow for a sizable production of the elements from Zn to Zr in NSE and by the α-process (not by the r-process). The model yields Ge, Sr, Y, and Zr in very good agreement with abundances of r-process deficient Galactic halo stars. A mild reduction of the minimum Y_e to $\sim$0.30–0.35, which cannot be excluded due to limited numerical resolution and the lack of the third dimension, leads to a weak r-process up to the silver region (Pd, Ag, and Cd), again well matching these elements in r-process deficient stars. The formation of heavy r-process nuclei requires Y_e to be as low as $\sim$0.15–0.20 and seems out of reach for our models.

We therefore determine ECSNe as an important source of Zn, Ge, As, Se, Br, Kr, Rb, Sr, Y, and Zr in the solar system and the early Galaxy. The frequency of ECSNe is constrained to $\sim$4% of all CCSN events on average over the Galactic history, but could have been higher at early Galactic epochs, compatible with the commonality of r-process deficient halo stars. Future, better resolved and in particular 3D models will have to elucidate the role of ECSNe as site of the weak r-process. Also important are new abundance studies of r-process deficient stars for more complete information on the elements from Zn to Zr and on weak r-process products between Nb and Cd.

We also investigated the effects of uncertainties in supernova dynamics as well as in nuclear reactions on the νp-process in the neutrino-driven outflows of CCSNe. Wind termination of the neutrino-driven outflow by collision with the preceding supernova ejecta causes a slowdown of the temperature decrease and thus plays a crucial role for the νp-process. The termination within the temperature range of $(1.5-3)\times10^9$ K (relevant to the νp-process) substantially enhances the efficiency of the p-nuclei production. This implies that the early wind phase with a termination radius of $\sim 200-500$ km is favored for the νp-process.

The νp-process also is highly sensitive to the electron fraction $Y_{e,3}$ (defined at 3×10^9 K) that controls the proton-to-seed ratio at the onset of the νp-process. An increase of only $\Delta Y_{e,3}\sim0.03$ results in $\Delta A_{max}\sim10$. The models with $Y_{e,3}=0.5-0.6$ (with the other parameters unchanged) produce sufficient amounts of the light p-nuclei up to $A=108$ (^{108}Cd). Furthermore, the models with $Y_{e,3}=0.60-0.65$ produce the p-nuclei up to $A=152$ (^{152}Gd). Note that this is a combined effect of the high $Y_{e,3}$ and the wind-termination at sufficiently high temperature (2.19×10^9 K in the standard model).

Variations on the triple-α and $^{56}\mathrm{Ni}(n,p)^{56}\mathrm{Co}$ reactions show great impact on the efficiency of the νp-process as well. Only a factor of two variation leads to a factor of 10 or more changes in the production of the p-nuclei with $A\sim100-110$. This is a consequence of the fact that the former and latter reactions control the seed (^{56}Ni) production and the strength of the nuclear flow starting from the seed nuclei.

Our results summarized above imply that, within possible ranges of uncertainties in supernova dynamics as well as in nuclear reactions, the solar inventory of the elements beyond iron up to Cd ($Z=48$) in the early convective ejecta of ECSNe as well as the p-nuclei up to $A=152$ (^{152}Gd) in the subsequent p-rich winds of more massive CCSNe could be explained. In other words, CCSNe, including their subset of ECSNe, are unlikely to be the origin of the heavy r-process elements ($A>120$). The heavy p-nuclei can be explained by the γ-process in the O/Ne layers of CCSNe. The origin of the heavy r-process nuclei should therefore be explored in different astrophysical phenomena, such as neutron star (or neutron star–black hole) binary mergers [46-52].

Acknowledgments
DFG grants EXC153, SFB/TR27, and SFB/TR7, and computing time at the NIC in Jülich, HLRS in Stuttgart, and the RZG in Garching are acknowledged.

References

[1] Meyer, B. S., Mathews, G. J., Howard, W. M., Woosley, S. E., & Hoffman, R. D. 1992, *Astrophys. J.*, 399, 656
[2] Woosley, S. E., Wilson, J. R., Mathews, G. J., Hoffman, R. D., & Meyer, B. S. 1994, *Astrophys. J.*, 433, 229
[3] Takahashi, K., Witti, J., & Janka, H.-T. 1994, *Astron. Astrophys.*, 286, 857
[4] Qian, Y. -Z. & Woosley, S. E. 1996, *Astrophys. J.*, 471, 331
[5] Otsuki, K., Tagoshi, H., Kajino, T., & Wanajo, S. 2000, *Astrophys. J.*, 533, 424
[6] Wanajo, S., Kajino, T., Mathews, G. J., & Otsuki, K. 2001, *Astrophys. J.*, 554, 578
[7] Thompson, T. A., Burrows, A., & Meyer, B. S. 2001, *Astrophys. J.*, 562, 887
[8] Prantzos, N., Hashimoto, M., Rayet, M., & Arnould, M. 1990, *Astron. Astrophys.*, 238, 455
[9] Rayet, M., Arnould, M., Hashimoto, M., Prantzos, N., & Nomoto, K. 1995, *Astron. Astrophys.*, 298, 517
[10] Hayakawa, T., Iwamoto, N., Kajino, T., Shizuma, T., Umeda, H., Nomoto, K. 2008, *Astrophys. J.*, 685, 1089
[11] Fischer, T., Whitehouse, S. C., Mezzacappa, A., Thielemann, F. -K., Liebendörfer, M. 2010, *Astron. Astrophys.*, 517, 80
[12] Hüdepohl, L., Müller, B., Janka, H. -Th., Marek, A., Raffelt, G. G 2010, *Phys. Rev. Lett.*, 104, 251101
[13] Wanajo, S., Janka, H.-T., & Müller, B. 2010c, *Astrophys. J. Lett*, submitted; arXiv1009.1000
[14] Fröhlich, C., et al. 2006a, *Astrophys. J.*, 637, 415
[15] Fröhlich, C., et al. 2006b, *Phys. Rev. Lett.*, 96, 142502
[16] Pruet, J., Hoffman, R. D., Woosley, S. E., Buras, R., & Janka, H. -Th. 2006, *Astrophys. J.*, 644, 1028
[17] Wanajo, S. 2006, *Astrophys. J.*, 647, 1323
[18] Wanajo, S., Janka, H.-T., & Kubono, S. 2010a, *Astrophys. J.*, submitted; arXiv1004.4487
[19] Wanajo, S., Nomoto, K., Janka, H.-T., Kitaura, F. S., Müller, B. 2009, *Astrophys. J.*, 695, 208
[20] Lattimer, J. M., & Swesty, F. D. 1991, *Nucl. Phys. A*, 535, 331
[21] Kitaura, F. S., Janka, H. -Th., & Hillebrandt, W. 2006, *Astron. Astrophys.*, 450, 345
[22] Janka, H.-Th., Müller, B., Kitaura, F. S., & Buras, R. 2008, *Astron. Astrophys.*, 485, 199
[23] Nomoto, K. 1987, *Astrophys. J.*, 322, 206
[24] Lodders, K. 2003, *Astrophys. J.*, 591, 1220
[25] Nomoto, K., Tominaga, N., Umeda, H., Kobayashi, C., & Maeda, K. 2006, *Nucl. Phys. A*, 777, 424
[26] Arlandini, C., Käppeler, F., Wisshak, K., Gallino, R., Lugaro, M., Busso, M., Straniero, O. 1999, *Astrophys. J.*, 525, 886
[27] Poelarends, A. J. T., Herwig, F., Langer, N., & Heger, A. 2008, *Astrophys. J.*, 675, 614
[28] Woosley, S. E. & Hoffman, R. D. 1992, *Astrophys. J.*, 395, 202
[29] Hartmann, D., Woosley, S. E., & El Eid, M. F. 1985, *Astrophys. J.*, 297, 837
[30] Honda, S., Aoki, W., Ishimaru, Y., Wanajo, S., & Ryan, S. G. 2006, *Astrophys. J.*, 643, 1180
[31] Honda, S., Aoki, W., Ishimaru, Y., & Wanajo, S. 2007, *Astrophys. J.*, 666, 1189
[32] Cowan, J. J., et al. 2005, *Astrophys. J.*, 627, 238
[33] Roederer, I. U., Sneden, C., Lawler, J. E., & Cowan, J. J. 2010, *Astrophys. J. Lett.*, 714, L123
[34] Sneden, C., et al. 2003, *Astrophys. J.*, 591, 936
[35] Wanajo, S. & Ishimaru, I. 2006b, *Nucl. Phys. A*, 777, 676
[36] Qian, Y. -Z. & Wasserburg, G. J. 2008, *Astrophys. J.*, 687, 272
[37] Wanajo, S., Itoh, N., Ishimaru, Y., Nozawa, S., & Beers, T. C. 2002, *Astrophys. J.*, 577, 853
[38] Wanajo, S. 2006c, *Astrophys. J. Lett.*, 650, L79
[39] Wanajo, S. 2007, *Astrophys. J. Lett.*, 666, L77
[40] Timmes, F. X. & Swesty, F. D. 2000, *Astrophys. J. Suppl.*, 126, 501
[41] Müller, B., Janka, H. -Th., & Dimmelmeier, H. 2010, *Astrophys. J. Suppl.*, 189, 104
[42] Buras, R., Rampp, M., Janka, H. -Th, & Kifonidis, K. 2006, *Astron. Astrophys.*, 447, 1049
[43] Arcones, A., Janka, H. -Th., & Scheck, L. 2006, *Astron. Astrophys.*, 467, 1227
[44] Kuroda, T., Wanajo, S., & Nomoto, K. 2008, *Astrophys. J.*, 672, 1068
[45] Weber, C., et al. 2008, *Phys. Rev. C*, 78, 054310
[46] Lattimer, J. M., Mackie, F., Ravenhall, D. G., & Schramm, D. N. 1977, *Astrophys. J.*, 213, 225
[47] Meyer, B. S. 1989, *Astrophys. J.*, 343, 254
[48] Freiburghaus, C., Rosswog, S., & Thielemann, F.-K. 1999, *Astrophys. J.*, 525, L121
[49] Goriely, S., Demetriou, P., Janka, H. -Th., Pearson, J. M., & Samyn, M. 2005, *Nucl. Phys. A*, 758, 587
[50] Surman, R., McLaughlin, G. C., Ruffert, M., Janka, H. -Th., & Hix, W. R. 2008, *Astrophys. J.*, 679, L117
[51] Metzger, B. D., et al. 2010 *Mon. Not. Royal Astron. Soc.*, 406, 2650
[52] Wanajo, S. & Janka, H.-T. 2010b, *The 10th International Symposium on Origin of Matter and Evolution of Galaxies: OMEG-2010. AIP Conference Proceedings*, 1269, 120; arXiv:1006.2277